WATER AVAILABILITY

Southern Hemisphere dominates recent decline in global water availability

Yongqiang Zhang[1]*†, Congcong Li[2,3]†, Francis H. S. Chiew[3], David A. Post[3], Xuanze Zhang[1], Ning Ma[1], Jing Tian[1], Dongdong Kong[4], L. Ruby Leung[5], Qiang Yu[2], Jiancheng Shi[6], Changming Liu[1]

Global land water underpins livelihoods, socioeconomic development, and ecosystems. It remains unclear how water availability has changed in recent decades. Using an ensemble of observations, we quantified global land water availability over the past two decades. We show that the Southern Hemisphere has dominated the declining trend in global water availability from 2001 to 2020. The significant decrease occurs mainly in South America, southwestern Africa, and northwestern Australia. In the Northern Hemisphere, the complex regional increasing and decreasing trends cancel each other, resulting in a negligible hemispheric trend. The variability and trend in water availability in the Southern Hemisphere are largely driven by precipitation associated with climate modes, particularly the El Niño-Southern Oscillation. This study highlights their dominant role in controlling global water availability.

Water availability over the global land is the net difference between water supply from precipitation and water demand from evapotranspiration (ET), thus representing streamflow and water storage change. Global land water availability influences livelihoods, socioeconomic development, and ecosystems (*1*–*3*) and could dramatically shift with climate change and socioeconomic growth as projected over the next several decades (*4*, *5*). In the past several decades, water availability has varied because of climate change that has intensified the hydrological cycle, vegetation greening that has increased terrestrial ET, and human water use that has altered streamflow (*6*). However, global land surface drought has changed little in the same period (*7*, *8*) because of complementary trends in precipitation and ET, which are controlled by multiple climate factors, such as available energy, humidity, and wind speed (*9*, *10*). Human activities have played a strong role in altering water availability by decreasing groundwater and streamflow, with potentially devastating effects on aquatic ecosystems and food production (*11*–*13*). Human-managed reservoirs have contributed 57% of the change in Earth's seasonal surface water storage variability. Human activities now drive 67% of the variability in surface water storage in the northern midlatitudes and nearly 100% in arid and semiarid regions (*5*). The observed trend in river flows can be explained only if anthropogenic climate change impact is included. Humans also influence the climate and affect the magnitude of river flows at regional and global scales (*14*). More than 70% of global net permanent water loss occurs in the Middle East and Central Asia, which is linked to drought and human activities, including damming, river diversion, and unregulated withdrawal (*15*). Global land surface could become drier because of the increasing trend in ET (*16*), particularly in the Northern Hemisphere, where vegetation greening (*17*) has controlled the decadal changes in ET (*18*, *19*). However, a recent study showed that vegetation greening could also increase water availability for approximately 45% of the global land surface (*20*) because the resulting moisture is recycled from vegetation to precipitation.

The above discussion highlights the conflicting conclusions that different studies have drawn about changes in water availability; there are several reasons for this. First, different periods are used in the different studies, varying from one to six decades (*1*, *7*, *21*, *22*). Second, different methods are used to estimate water availability changes; for example, some studies use water storage changes from Gravity Recovery and Climate Experiment (GRACE) satellite observations to reflect changes in water availability (*22*), whereas other studies use the climate drought severity index, potential ET (*7*, *23*, *24*), or river flow (*14*, *25*, *26*) to indicate water availability changes. Without large-scale validations against observations across the global land surface, water availability changes estimated using different approaches are questionable.

In this study, we analyzed the past two decades to elucidate changes in water availability across the globe and their causality. We validated the water availability trend using a consistent method against GRACE satellite and streamflow observations. We used precipitation minus ET (P – ET) to estimate water availability on the land surface and assumed that the trend in P – ET in a river basin is identical to the trend of water storage change plus streamflow at monthly to decadal scales. We combined multiple remote sensing and ground-based precipitation and ET datasets using simple model output averaging (SMA), Bayesian model averaging (BMA), and machine learning (ML) and developed an ensemble estimate for this study (materials and methods). The ensemble mean annual P – ET trend compares well [coefficient of determination (R^2) = 0.81] with the trend observed (water storage change plus streamflow) from 2003 to 2016 in 134 river basins that cover 36% of the global land surface (figs. S1 to S6 and table S1).

Interannual variability and trend

The annual anomaly of water availability across global land surface from 2001 to 2020 varies from −30 mm year^{-1} to +22 mm year^{-1}, with an annual variance of 146 mm^2 year^{-2} (Fig. 1A). The interannual variability in global water availability is largely contributed by the Southern Hemisphere. Despite accounting for only 26% of the global land area (not including Antarctica), the Southern Hemisphere contributes 43 ± 2.6% of the total global water availability interannual variability with its variance and 19 ± 3.9% with the covariance between the two hemispheres removed. The Northern Hemisphere, accounting for 74% of the global land area, contributes 38 ± 2.4% of the global water availability variance.

The global land water availability declined from 2001 to 2020, with a trend of −0.96 ± 0.27 mm year^{-2} ($P < 0.05$, table S2). The water availability across the Southern Hemisphere decreased significantly (−3.55 ± 0.71 mm year^{-2}, $P < 0.05$), but there was little trend in water availability across the Northern Hemisphere (−0.05 ± 0.12 mm year^{-2}). The percentage contributions from the Southern Hemisphere and the Northern Hemisphere are 95.2 ± 5.6% and 4.8 ± 5.6%, respectively. The Southern Hemisphere therefore dominated the global declining water availability trend from 2001 to 2020, despite its much smaller land surface area (Fig. 1, B and C). Over the Northern Hemisphere, water availability increased in southern China, eastern North America, and northeastern Asia and decreased in mainland southeast Asia, eastern Europe, and large parts of Siberia (Fig. 1B and fig. S7). The increasing and decreasing water availability trends in the different regions cancel each other, resulting in little trend when aggregated over the Northern Hemisphere. In the Southern Hemisphere, a strong decreasing trend is observed in South America ($P < 0.01$), the majority of Africa, and central and northwestern Australia ($P < 0.05$) (Fig. 1B). Nevertheless, there are some regions, such as the southern part of South America, that show a significant increasing trend ($P < 0.05$).

[1]Key Laboratory of Water Cycle and Related Land Surface Processes, Institute of Geographic Sciences and Natural Resources Research, Chinese Academy of Sciences, Beijing 100101, China. [2]State Key Laboratory of Soil Erosion and Dryland Farming on the Loess Plateau, Institute of Soil and Water Conservation, Northwest A&F University, Yangling 712100, China. [3]CSIRO Environment, Black Mountain, Canberra, ACT 2601, Australia. [4]Department of Atmospheric Science, School of Environmental Studies, China University of Geosciences, Wuhan, China. [5]Pacific Northwest National Laboratory, Richland, WA 99352, USA. [6]National Space Science Center, Chinese Academy of Sciences, Beijing 100190, China.
*Corresponding author. Email: zhangyq@igsnrr.ac.cn
†These authors contributed equally to this work.

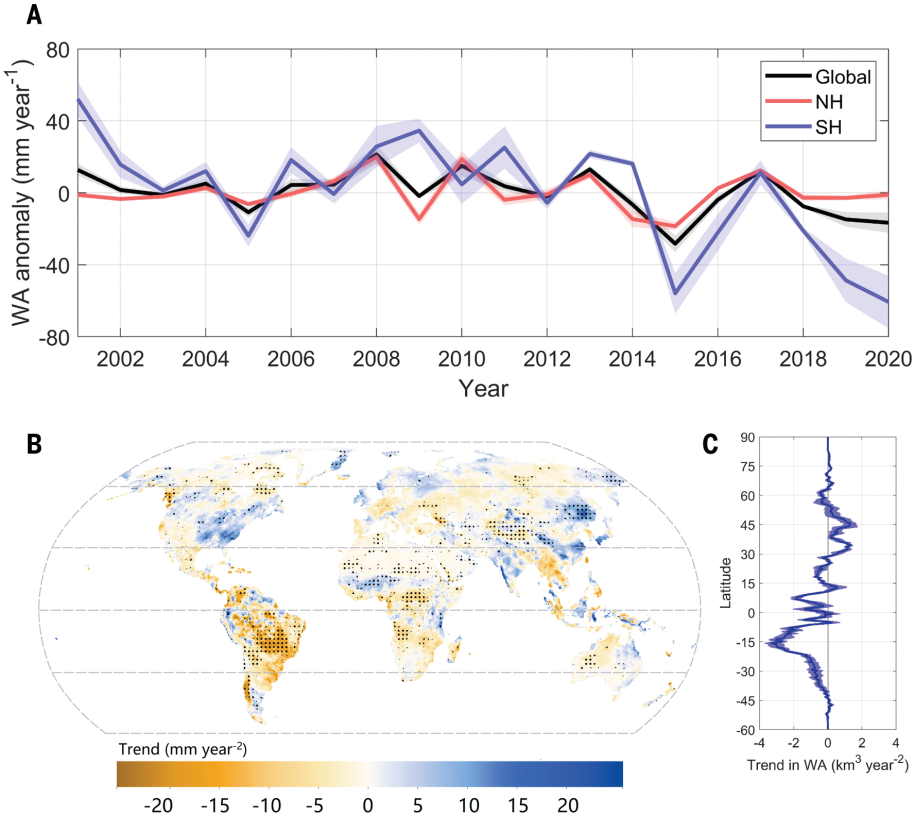

Fig. 1. Annual time series, variability, and trend of global land water availability (WA). (**A**) Annual time series of land WA across the globe (black), Northern Hemisphere (NH, red), and Southern Hemisphere (SH, blue). (**B**) Trend in WA at each 0.5° by 0.5° grid cell across the globe from 2001 to 2020. Stippling indicates that the trend is statistically significant at $P < 0.05$. (**C**) Aggregated trend in WA along each 0.5° latitude band (km^3 year^{-2}). The solid line and shading denote the mean and 1 SD of three estimates [simple model output (SMA) averaging, Bayesian model averaging, and machine learning], respectively.

Attribution and causality

The interannual variability of water availability in about 50% of the global land surface is dominated by precipitation (with a relative contribution ratio of variance in water availability > 0.6) (fig. S8). This is also the case for the trend in water availability in wet regions such as eastern China, northeastern Asia, Amazonia, eastern North America, and Europe (Fig. 2A and fig. S9). Conversely, in very dry regions such as the Sahara, central Asia, central Australia, and western United States, the trend in water availability is driven by the trend in ET or in both ET and precipitation (Fig. 2A and fig. S9). The spatial pattern of Fig. 2A is quantitively analyzed by using the correlation between the precipitation contribution (or ET contribution) and aridity index (Fig. 2, B and C), with correlation coefficient (r) = 0.41 ($P < 0.001$) and r = 0.33 ($P < 0.001$) across the land surface of the Northern Hemisphere and Southern Hemisphere, respectively. This analysis demonstrates the tendency for a higher precipitation contribution in wetter grid cells with a higher aridity index (Fig. 2, B and C).

The relationship between the precipitation contribution and the aridity index is further supported by the water availability trends in 40 large river basins (Fig. 2, D and E). Precipitation dominates the water availability trend in wetter basins such as the Saint Lawrence, Amazon, Mississippi, and Yangtze, whereas ET dominates the water availability trend in drier basins such as the Ob, Colorado, Okavango, and Tarim. Both precipitation and ET contribute to the water availability trend in some basins, such as the Yellow, Indus, Ganges, and Mekong (Fig. 2D). Strong trends in water availability are generally observed in basins where either precipitation or ET dominates the trend, and little trend is found in basins where precipitation and ET contribute more evenly. Both positive and negative water availability trends are observed where precipitation dominates, but the water availability trend is generally negative where ET dominates (Fig. 2, D and E).

There is a strong positive correlation between the annual water availability and the Southern Oscillation Index (SOI) in southeast Asia, the equatorial Pacific, Australia, central America, and northern South America (Fig. 3A). The SOI is the difference between surface air pressure in Tahiti and Darwin. Positive SOI values indicate La Niña conditions, and hence, a positive correlation indicates wetter conditions in the aforementioned regions during La Niña and drier conditions during El Niño. The water availability-El Niño-Southern Oscillation (ENSO) correlation here has also been observed for individual water cycle components, such as precipitation (*27*, *28*) and river flow (*29*).

In the Southern Hemisphere, regions with positive correlations between water availability and SOI largely show decreasing or insignificant water availability trends from 2001 to 2020 (Fig. 3B). By contrast, areas with negative water availability-SOI correlations display a tendency for increasing water availability trends in both the Northern and Southern Hemispheres (Fig. 3B).

There is no clear relationship between the water availability trend and the aridity index in the Northern Hemisphere (Fig. 3C). In the Southern Hemisphere, there is a relatively weak but statistically significant correlation between the water availability trend and the aridity index, with larger decreasing trends in wetter regions ($r = -0.19$, $P < 0.001$) (Fig. 3C). This observed "wet gets drier" water availability change from 2001 to 2020 is opposite to the "dry gets drier, wet gets wetter" hydrological change postulated under global warming.

There were significant increases ($P < 0.05$) in the leaf area index (LAI) or greening over large areas of the Northern Hemisphere from 2001 to 2020, especially in eastern China, India, and Europe (figs. S10 and S11). To investigate whether greening plays a role in the water availability and aridity index relationship, we separated the regions with increasing or decreasing LAI trends (Fig. 3C). In the Northern Hemisphere, there is no relationship between the water availability trend and the aridity index, and greening has little or no influence on the relationship. In the Southern Hemisphere, the statistically significant relationship between the water availability trend and the aridity index is stronger in grid cells that show an increasing LAI trend ($r = -0.27$, $P < 0.001$) (Fig. 3C). These results suggest that the large-scale greening in some parts of the Northern Hemisphere was accompanied by both increases and decreases in water availability, depending on the region. In the Southern Hemisphere, greening has accentuated the decline in water availability driven by the decline in precipitation (Fig. 2A), likely because greening further reduces water availability by increasing ET.

Discussion and implication

This study demonstrates that the interannual variability and trends in global water availability from 2001 to 2020 are largely dominated

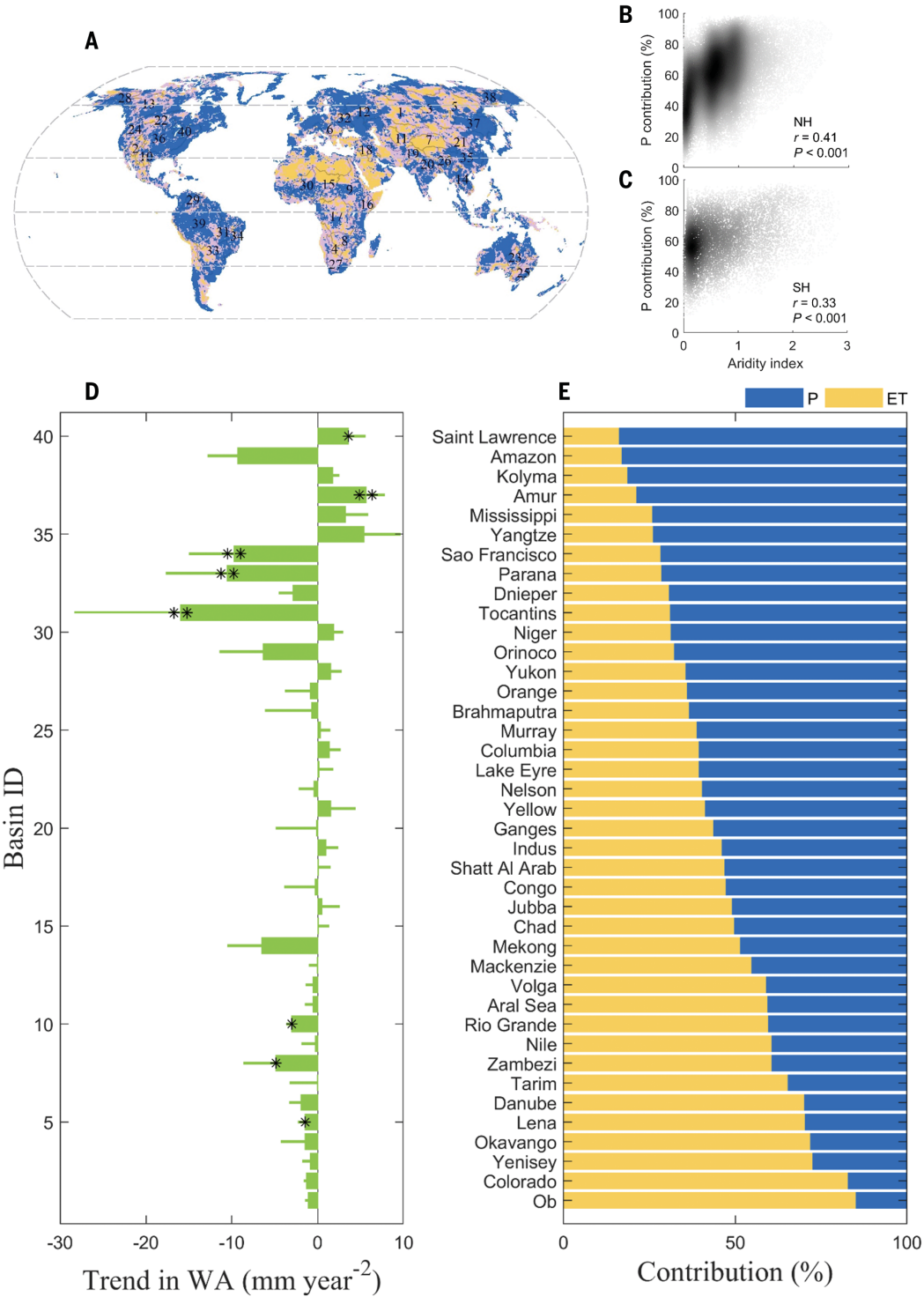

Fig. 2. Relative contribution of precipitation (P) and actual evapotranspiration (ET) to the trends in WA from 2001 to 2020. (**A**) Contribution across each grid cell. Blue indicates that P dominates (with a contribution larger than 60%), orange indicates that actual ET dominates (with a contribution larger than 60%), and purple means that both P and ET play an important role (both with a contribution of 40 to 60%). (**B**) Scatterplots of the P contribution to the water availability (WA) trend in each grid cell versus the aridity index (mean annual P divided by mean annual potential ET) for grid cells in the NH. A higher aridity index indicates a wetter climate. Darker regions have a higher density of points and cells. (**C**) Same as (B) except that the grid cells indicate the SH. (**D**) Aggregated trend for 40 large river basins, with each bar representing the mean (±1 SD) from nine estimates. *P < 0.1; **P < 0.05. (**E**) P and ET contributions to the WA trend in the 40 river basins. The results presented from (A) to (E) are for the SMA WA estimate (materials and methods).

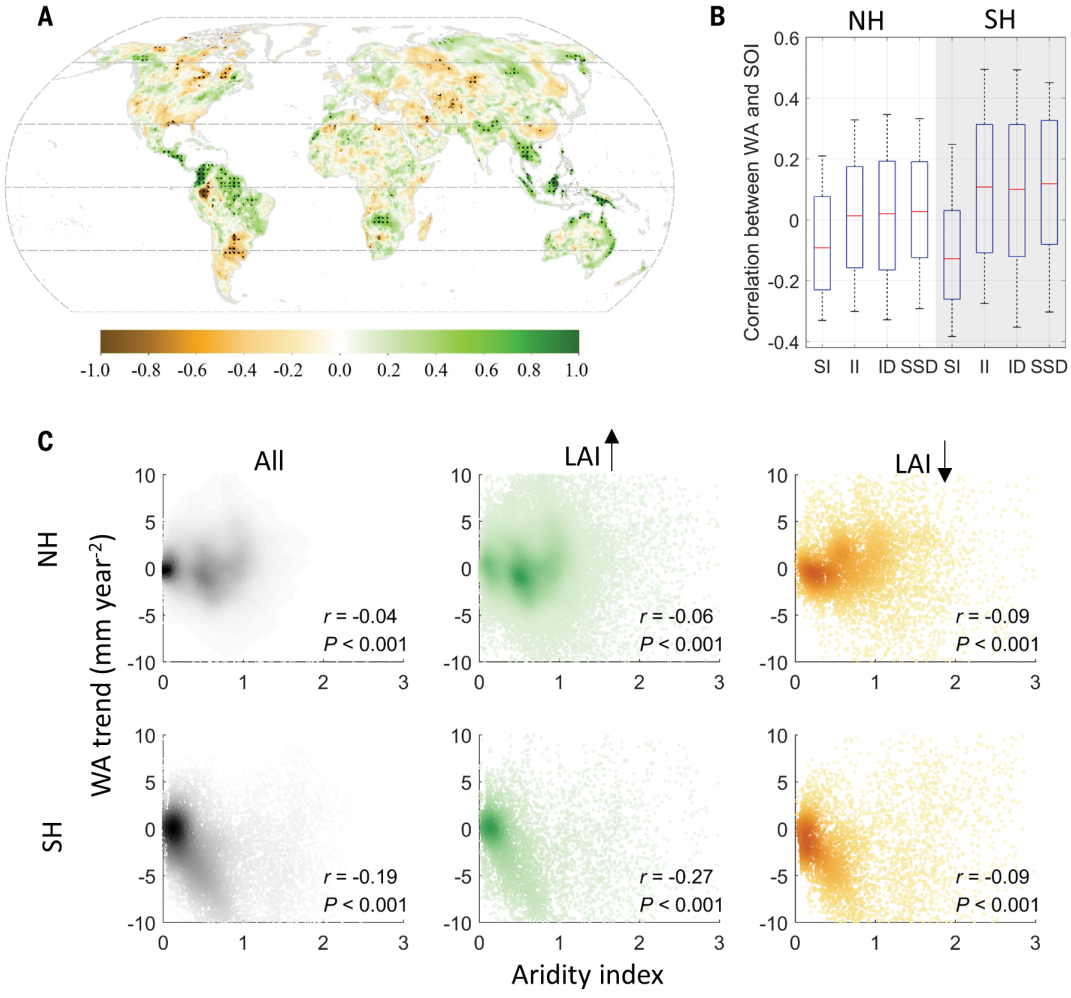

Fig. 3. Causality for interannual variability and trends in WA. (**A**) Correlation between annual WA and annual SOI from 2001 to 2020 at each 0.5° by 0.5° grid cell. Stippling indicates that the correlation is statistically significant ($P < 0.05$). (**B**) Correlation between WA and SOI grouped by different WA trend categories. For each boxplot, the bottom, middle, and top of the box are the 25th, 50th, and 75th percentiles, respectively, and the bottom and top whiskers show the 10th and 90th percentiles, respectively. SI, II, ID, and SSD indicate statistically significant increases in water availability ($P \leq 0.05$), nonstatistically significant increases in WA, nonstatistically significant decreases in WA, and statistically significant decreases in WA ($P \leq 0.05$), respectively, for the NH (white area) and the SH (gray area). (**C**) (Left) Scatterplots of trend versus aridity index for all grid cells, (middle) grid cells with increasing LAI, and (right) grid cells with decreasing LAI for the NH (top panels) and SH (bottom panels).

by the variability and trend in the Southern Hemisphere. The latter are largely dependent on the hydroclimate region and are linked to regional climate, natural variability of precipitation, and large-scale circulation drivers of changes in precipitation and ET, such as those related to the climate modes and vegetation greening (Fig. 4). The decline in water availability over large parts of the Southern Hemisphere in the relatively short 20-year period that we analyzed could be related to complex changes in climate modes and/or their relationships with precipitation, such as increasing ENSO-rainfall variability in a warming Earth (*27*, *30*, *31*) and changes in large-scale meridional circulations, such as the expanding Hadley cell (*32*, *33*). Among the various climate modes, ENSO is particularly important because it induces interannual variability in precipitation and water availability in large parts of the Southern Hemisphere and equatorial Pacific, with high water availability during La Niña and low water availability during El Niño. The ENSO roles are further corroborated by analyzing the correlations between water availability and the Niño 3.4 Index—another commonly used index (fig. S12)—and over a longer period from 1983 to 2020, confirming that the precipitation versus ENSO correlation in the Southern Hemisphere was stronger than that in the Northern Hemisphere (fig. S13). In addition, the expansion of the Hadley cell could be an important factor contributing to the drying in the Southern Hemisphere because this expansion pushes the winter storm tracks further south, away from the land masses and into the Southern Ocean (*33*, *34*). Notably, the Coupled Model Intercomparison Project Phase 5 (CMIP5) and CMIP6 models project a poleward shift of the Hadley cell edge that is about two to three times as large in the Southern Hemisphere as it is in the Northern Hemisphere (*35*).

The complex trends in water availability in the Northern Hemisphere can be partly related to direct and indirect human activities (Fig. 4). Irrigation can alter water availability regionally, but its role is secondary compared with natural climate variability and changes in precipitation and ET (*36*). For example, in the northern midlatitudes (16° to 22° and 35° to 42°), irrigation and greening may have contributed to the decreasing trend in water availability. Both LAI and water availability have largely increased, suggesting that vegetation greening may be

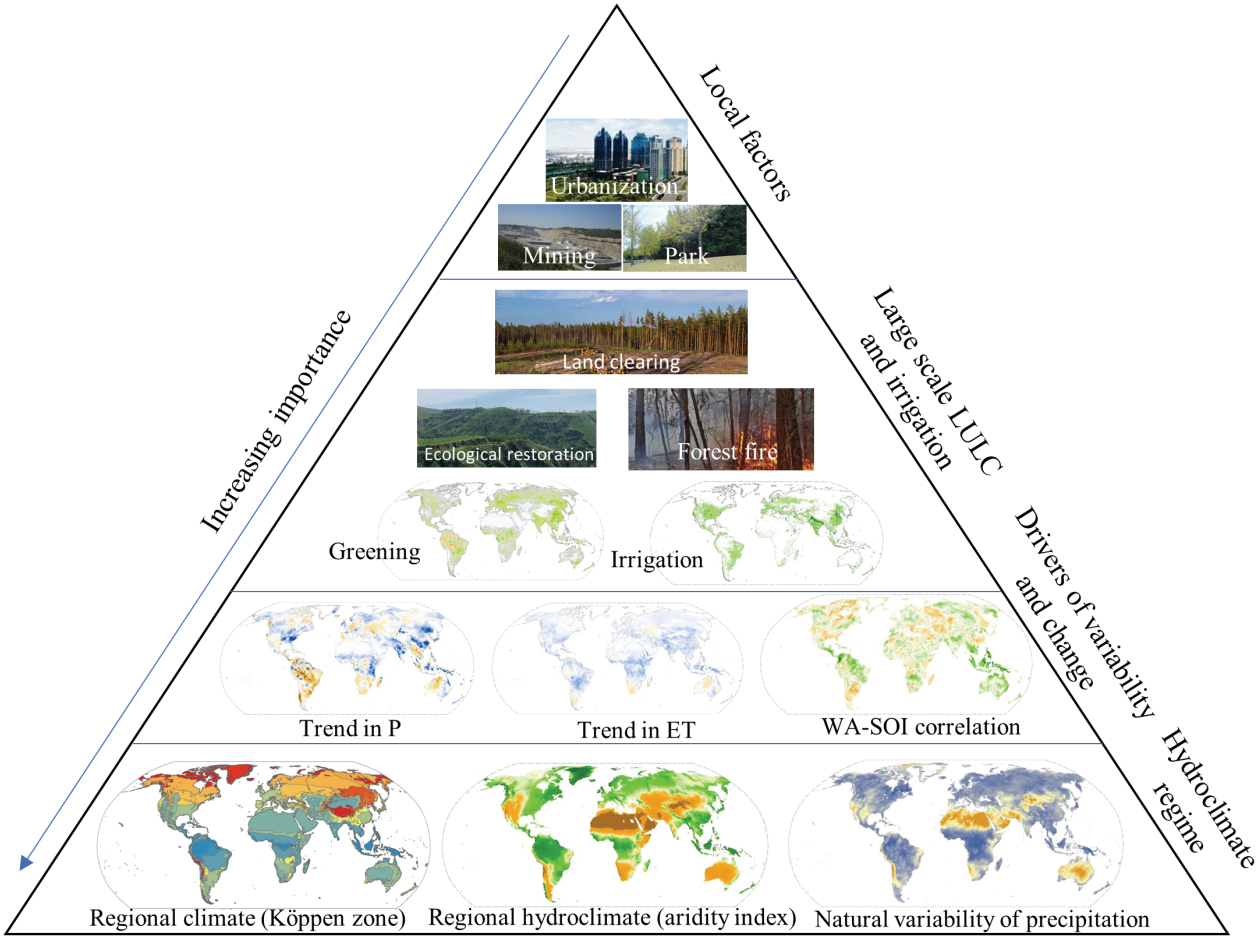

Fig. 4. Conceptualized understanding of major factors controlling variability and trends in WA. Natural variability of precipitation in the lower-right panel is expressed as the coefficient of variation of precipitation, the ratio of the SD of annual precipitation to the annual mean. LULC, land use and land cover.

positively coupled with regional water availability (*20*) (fig. S11). Therefore, greening could be a water availability driver (negative effect) and/or a response variable of water availability (positive effect), particularly in the northern midlatitudes, where both greening and water availability are strongly influenced by anthropogenic activities. Therefore, vegetation changes and large-scale irrigation can play a secondary role in controlling regional water availability (Fig. 4).

Our study has broad implications. First, it is crucial for water-resource managers to understand the dominant factors controlling interannual variability and trends in water availability. Precipitation has dominated the variability and trends in water availability, especially in the Southern Hemisphere, such as in South America and Australia, where river flow has been projected to continue to decline under climate change (*37*). Vegetation changes and irrigation, which are correlated in the irrigated regions, can play secondary roles at small to regional scales. Second, in terms of ecohydrology, vegetation greening could reduce local water availability, but our findings indicate that its large-scale impact is relatively weak. Vegetation greening can arise not only from an increase in precipitation but also from direct anthropogenic interventions, such as ecological restoration to mitigate land degradation and irrigation to enhance food production (*17*). Moreover, it fosters moisture recycling by increasing precipitation (*38*), indicating a coevolution of vegetation greening and water availability in the Northern Hemisphere. However, it is difficult to disentangle the interactions between vegetation and water availability despite recent efforts in modeling (*20*, *39*, *40*). Third, in many parts of the world, especially in wet regions such as the Amazon, ET plays a relatively minor role in determining water availability trends. Fourth, water availability provides a fundamental water source for carbon and nutrient cycles in ecosystems across the global land surface (*41*). Therefore, our results provide some indication for trends in vegetation growth (*42*), carbon, and other nutrients, including regional declining trends in the carbon cycle in Amazonia (*43*). Last, our results and conclusions pertain to the past two decades and thus can at least provide a constraint for global models driven by the observed sea surface temperature variability.

It remains challenging to determine and interpret water availability trends and their drivers over a longer period before 2000 because large basin-scale validation data are not available and because robust and consistent remotely sensed ET estimates are available only for the recent decades (*44*). Fusion of observations and global model simulations, including multimodel ensembles and large-ensemble simulations, can potentially reduce uncertainty in estimating water availability over a longer period.

REFERENCES AND NOTES

1. P. C. D. Milly, K. A. Dunne, A. V. Vecchia, *Nature* **438**, 347–350 (2005).
2. T. Oki, S. Kanae, *Science* **313**, 1068–1072 (2006).
3. M. Jung *et al.*, *Nature* **541**, 516–520 (2017).
4. Y. Pokhrel *et al.*, *Nat. Clim. Chang.* **11**, 226–233 (2021).
5. S. W. Cooley, J. C. Ryan, L. C. Smith, *Nature* **591**, 78–81 (2021).
6. G. Villarini, C. Wasko, *Nat. Clim. Chang.* **11**, 725–726 (2021).
7. J. Sheffield, E. F. Wood, M. L. Roderick, *Nature* **491**, 435–438 (2012).
8. P. Greve *et al.*, *Nat. Geosci.* **7**, 716–721 (2014).
9. X. Lian *et al.*, *Nat. Rev. Earth Environ.* **2**, 232–250 (2021).

10. T. R. McVicar *et al*., *J. Hydrol.* **416–417**, 182–205 (2012).
11. M. O. Cuthbert *et al*., *Nature* **572**, 230–234 (2019).
12. C. Dalin, Y. Wada, T. Kastner, M. J. Puma, *Nature* **543**, 700–704 (2017).
13. I. E. M. de Graaf, T. Gleeson, L. P. H. (Rens) van Beek, E. H. Sutanudjaja, M. F. P. Bierkens, *Nature* **574**, 90–94 (2019).
14. L. Gudmundsson *et al*., *Science* **371**, 1159–1162 (2021).
15. J. F. Pekel, A. Cottam, N. Gorelick, A. S. Belward, *Nature* **540**, 418–422 (2016).
16. Y. Zhang *et al*., *Sci. Rep.* **6**, 19124 (2016).
17. C. Chen *et al*., *Nat. Sustain.* **2**, 122–129 (2019).
18. Y. Yang *et al*., *Nat. Rev. Earth Environ.* **4**, 626–641 (2023).
19. C. Li, Y. Zhang, Y. Shen, Q. Yu, *Sci. Bull.* **65**, 1859–1861 (2020).
20. J. Cui *et al*., *Nat. Geosci.* **15**, 982–988 (2022).
21. M. Jung *et al*., *Nature* **467**, 951–954 (2010).
22. M. Rodell *et al*., *Nature* **557**, 651–659 (2018).
23. P. C. D. Milly, K. A. Dunne, *Nat. Clim. Chang.* **6**, 946–949 (2016).
24. A. Dai, *Nat. Clim. Chang.* **3**, 52–58 (2013).
25. Y. Yang *et al*., *Water Resour. Res.* **54**, 4700–4713 (2018).
26. J. S. Mankin, R. Seager, J. E. Smerdon, B. I. Cook, A. P. Williams, *Nat. Geosci.* **12**, 983–988 (2019).
27. A. Timmermann *et al*., *Nature* **559**, 535–545 (2018).
28. S. Power, F. Delage, C. Chung, G. Kociuba, K. Keay, *Nature* **502**, 541–545 (2013).
29. R. Emerton *et al*., *Nat. Commun.* **8**, 14796 (2017).
30. K.-S. Yun *et al*., *Commun. Earth Environ.* **2**, 43 (2021).
31. P. Huang, S.-P. Xie, *Nat. Geosci.* **8**, 922–926 (2015).
32. V. B. P. Chagas, P. L. B. Chaffe, G. Blöschl, *Nat. Commun.* **13**, 5136 (2022).
33. D. J. Seidel, Q. Fu, W. J. Randel, T. J. Reichler, *Nat. Geosci.* **1**, 21–24 (2008).
34. S.-Y. Kim *et al*., *Sci. Adv.* **9**, eadg1801 (2023).
35. K. M. Grise, S. M. Davis, *Atmos. Chem. Phys.* **20**, 5249–5268 (2020).
36. Z. Huang, X. Yuan, X. Liu, *J. Hydrol.* **601**, 126648 (2021).
37. Y. Zhang *et al*., *Nat. Water* **1**, 261–271 (2023).
38. R. J. van der Ent, H. H. G. Savenije, B. Schaefli, S. C. Steele-Dunne, *Water Resour. Res.* **46**, W09525 (2010).
39. S. Zhou *et al*., *Nat. Clim. Chang.* **11**, 38–44 (2021).
40. G. Miguez-Macho, Y. Fan, *Nature* **598**, 624–628 (2021).
41. A. Ahlström *et al*., *Science* **348**, 895–899 (2015).
42. W. Li *et al*., *Nat. Commun.* **13**, 3959 (2022).
43. L. V. Gatti *et al*., *Nature* **595**, 388–393 (2021).
44. Y. Zhang *et al*., *Remote Sens. Environ.* **222**, 165–182 (2019).

ACKNOWLEDGMENTS

Y.Q.Z. acknowledges support from the Chinese Academy of Sciences. C.C.L. thanks the Chinese Scholarship Council for financial support. F.H.S.C., D.A.P., and C.C.L. acknowledge support from the Australian Commonwealth Scientific and Industrial Research Organisation. The streamflow data used for the study were obtained from the Global Runoff Data Centre (GRDC), the US Geological Survey (USGS) National Water Information System and Geospatial Attributes of Gages for Evaluating Streamflow (GAGES)-II database, the Australian Bureau of Meteorology, and the *Chinese River Sediment Bulletin*. **Funding:** The study was supported by the National Key R&D Program of China (grant no. 2022YFC3002804), the National Natural Science Foundation of China (grant nos. 41971032 and 42330506), and the Second Tibetan Plateau Scientific Expedition and Research Program (2019QZKK020807 and 2019QZKK0206). **Author contributions:** Y.Q.Z. designed the study and wrote the first draft. C.C.L. collated most of the datasets and conducted the data analysis and model simulations. Y.Q.Z. and C.C.L. prepared the figures. F.H.S.C. and D.A.P. provided critical insights into the data analysis. N.M. contributed to the collation of the streamflow dataset. D.D.K. collated and processed the leaf area index dataset. All authors contributed to discussion, text revisions, and interpretations of the results. **Competing interests:** The authors declare that they have no competing interests. **Data and materials availability:** Data and code are stored in the Figshare repository at https://doi.org/10.6084/m9.figshare.23949225.

SUPPLEMENTARY MATERIALS

science.org/doi/10.1126/science.adh0716
Materials and Methods
Supplementary Text
Figs. S1 to S14
Tables S1 and S2
References (*45*–*65*)

Submitted 8 February 2023; accepted 11 September 2023
10.1126/science.adh0716

Southern Hemisphere dominates recent decline in global water availability

Yongqiang Zhang, Congcong Li, Francis H. S. Chiew, David A. Post, Xuanze Zhang, Ning Ma, Jing Tian, Dongdong Kong, L. Ruby Leung, Qiang Yu, Jiancheng Shi, and Changming Liu

Science **382** (6670), . DOI: 10.1126/science.adh0716

Editor's summary

How has climate change affected the availability of land water over the recent past? Zhang *et al*. calculate global land water availability over the last two decades and found an overall decline that has been dominated by a negative trend in the Southern Hemisphere, whereas a mixture of positive and negative regional trends in the Northern Hemisphere have led to no significant change there (see the Perspective by Blöschl and Chaffe). El Niño is the most important climate mode affecting water availability in the Southern Hemisphere. —H. Jesse Smith